Global-scale random bottom pressure fluctuations from oceanic intrinsic variability

Mengnan Zhao, Rui Ponte, Thierry Penduff

ATMOSPHERIC SCIENCE

Global-scale random bottom pressure fluctuations from oceanic intrinsic variability

Mengnan Zhao[1], Rui M. Ponte[1]*, Thierry Penduff[2]

Intrinsic processes such as mesoscale turbulence have recently been proved as important as atmospheric variability in causing variations in ocean bottom pressure (p_b). Intrinsic processes are also known to generate random variability on scales larger than the mesoscale through inverse energy cascades or large-scale baroclinic instability. Here, model analyses reveal a truly global-scale, intrinsic p_b mode of variability at monthly time scales that relies on a different mechanism. The intrinsic mode has largest amplitudes around Drake Passage and opposite polarity between the Southern Ocean and Atlantic/Arctic oceans. Its signature is consistent with localized eddy-driven p_b anomalies of opposite sign near Drake Passage that then adjust freely in the rest of the ocean via barotropic wave processes. This intrinsic mode seems consistent with observed p_b variability.

INTRODUCTION

Ocean bottom pressure (p_b) provides an important metric to evaluate the global ocean mass distribution, which can change due to freshwater fluxes from the land and atmosphere and redistribution by the ocean circulation and tides (*1*). Better understanding of p_b and its dynamics provides insights on sea level changes, ocean circulation patterns, heat and freshwater budgets, and more generally on climate (*2*–*4*).

Global-scale measurements of p_b variations are available since the launch of the Gravity Recovery and Climate Experiment (GRACE) and its follow-on (GRACE-FO) satellites (*5*–*8*). Effective interpretations of p_b fields derived from these missions are essential for their proper assimilation in ocean models (*9*, *10*) and to better understand dynamics associated with p_b in relation to other climate variables.

Variations in p_b occur over a wide range of spatiotemporal scales, reaching thousands of kilometers. Many past studies thus implicitly assume that large-scale p_b variations are mostly a response to atmospheric fluctuations (*11*–*13*). Variations in p_b not only can indeed be forced directly by the atmospheric variability (e.g., surface wind stress) but can also emerge spontaneously from oceanic intrinsic processes (*14*, *15*); one thus needs to distinguish between forced and intrinsic bottom pressure variations (respectively denoted as p_b^f and p_b^i hereafter).

Nonlinear mesoscale (or smaller scale) turbulence is the best-known example of these intrinsic processes, which generate random p_b^i variations at spatial scales of order 100 km and time scales of weeks to months. However, recent modeling studies have shown that p_b^i variations could be as important as those of p_b^f at scales of order 1000 km (*13*, *16*). In the intra-annual frequency band, p_b^i can actually be larger than p_b^f in almost a quarter of the ocean area (*16*).

Two main processes have been proposed to explain the existence of intrinsic variability at large spatiotemporal scales. One process involves a spatiotemporal inverse energy cascade, in which the kinetic energy of mesoscale turbulence nonlinearly feeds larger spatial and longer time scales (*17*–*19*). Another process is large-scale baroclinic instability, where horizontal density gradients of the general circulation feed large-scale random intrinsic variability (*20*, *21*). The present study reveals a truly global-scale mode of p_b^i variability that involves a different mechanism to attain its coherence across several ocean basins.

RESULTS

Global-scale p_b^i pattern

Disentangling p_b^i and p_b^f variability is barely possible from observational data or from the output of single-model simulations. Here, we take advantage of the large ensemble of eddy-permitting global ocean/sea-ice simulations from the Oceanic Chaos-Impacts, Structure, Predictability (OCCIPUT) project (*22*, *23*). A total of 50 ensemble members were initialized from a 21-year common spin-up, and then, they were driven between 1960 and 2015 by the same atmospheric forcing derived from the ERA-Interim atmospheric reanalysis (*22*). As explained in (*22*) and detailed in (*24*, *25*), these stochastic perturbations slightly affect density gradients, hence geostrophic velocities, within each member during year 1960; they trigger the growth of the ensemble spread, whose subsequent saturation and evolution is solely controlled by the unperturbed ocean dynamics. This ensemble yields 50 distinct realizations of this 56-year oceanic evolution and, particularly, of daily p_b^i variability. Over most of the oceans, an ensemble of 50 members is sufficient to distinguish forced from intrinsic variability (*23*, *26*).

The daily p_b signals are averaged to monthly fields and within $3^\beta \times 3^\beta$ cells to smooth out mesoscale features. The $3^\beta \times 3^\beta$ cells are chosen to be consistent with GRACE data resolution, which allows for more convenient comparison and interpretation. At a given location and month, the forced signal p_b^f is estimated by the ensemble mean of p_b, and the intrinsic signal p_b^i is derived from each ensemble member by subtracting p_b^f from p_b, giving 50 realizations of the p_b^i field.

To identify any potential large-scale spatial pattern, we apply empirical orthogonal function (EOF) decomposition to each of the 50 p_b^i fields. We find a common leading EOF spatial pattern (mode 1 hereafter), with small SD over all ensemble members

[1]Atmospheric and Environmental Research Inc., Lexington, MA, USA. [2]Université Grenoble Alpes, CNRS, INRAE, IRD, Grenoble INP, Institut des Géosciences de l'Environnement (IGE), Grenoble, France.
*Corresponding author. Email: rponte@aer.com

(Fig. 1). (Note that the leading EOF spatial patterns for different members could show opposite signs. Signs of the EOF patterns were made consistent before computing the ensemble average shown in Fig. 1A.) The common mode 1 explains, on average, 20.3% (±1.6%) of p_b^i variance over all ensemble members. The p_b^i variations in mode 1 exhibit a global-scale signature with out-of-phase behavior between the Southern Ocean and the Atlantic/Arctic oceans, where the EOF loading is largest (Fig. 1A), and are most prominent on monthly time scales (fig. S1).

The amplitude of p_b^i mode 1 reaches values of more than 1 cm in the Southern Ocean, with largest values around the Drake Passage region and some evidence for trapping of energy to the Antarctic coast, and very uniform values of several millimeters in the Atlantic and Arctic oceans (Fig. 1A). To quantify the importance of this global-scale p_b^i pattern relative to other variability, we examine the ratio of the temporal SD of p_b^i from mode 1 to those of total p_b^i and p_b^f for an arbitrary ensemble member (Fig. 2). (Results are not sensitive to the choice of ensemble member.) In the basins with largest amplitudes, mode 1 can amount to more than 80% of total p_b^i variability (Fig. 2A) and more than 50% of total p_b^f variability (Fig. 2B), indicating the importance of the global scale p_b^i pattern highlighted in Fig. 1A for explaining p_b variability in vast areas of the ocean.

Origin of the global-scale p_b^i pattern

The emergence of a coherent pattern of p_b^i variability on the planetary scale from nonlinear mesoscale processes would be unexpected. Although inverse cascade processes do not set a formal limit on the largest scales to which small-scale energy can be transferred (*18*, *19*), it is highly unlikely that these processes would give rise to some of the mode 1 features seen in Fig. 1 (e.g., homogeneous amplitudes within most basins but quite different across basins and with a clear global bipolar structure). Similar issues arise if one considers an explanation in terms of large-scale baroclinic instabilities, which also typically give rise to variability at (multi-)decadal scales (*20*, *21*) compared to the mostly subannual variability associated with mode 1 (fig. S1). Instead, the spatial character of mode 1 suggests a much more plausible interpretation, in terms of local generation of relatively small-scale p_b^i anomalies, which then lead to a "free" barotropic adjustment over the global ocean.

Figure 1 shows the strongest amplitudes of mode 1 occur in regions near the Drake Passage, including the Bellingshausen-Amundsen basin and the Patagonian shelf. (There is also a maximum in the Agulhas retroflection region, but as per Fig. 1B, the amplitude of mode 1 in that region is more uncertain across the ensemble.) Moreover, the structure across Drake Passage is bipolar. Our interpretation is that relatively short-scale nonlinear processes generate relatively large p_b^i anomalies of opposite sign across Drake Passage and that these localized anomalies constitute the main driving for the global mode. The p_b^i signals in the rest of the ocean are essentially freely evolving barotropic adjustments to the p_b^i anomalies across Drake Passage.

Anomalies to the west of Drake Passage adjust westward along H/f contours (H is water depth, and f is Coriolis parameter; Fig. 1A), which define pathways of propagation of oceanic barotropic Rossby waves (*27*, *28*) around Antarctica. In addition to Rossby-type barotropic adjustment, westward propagating Kelvin waves around this continent may also be involved. This adjustment

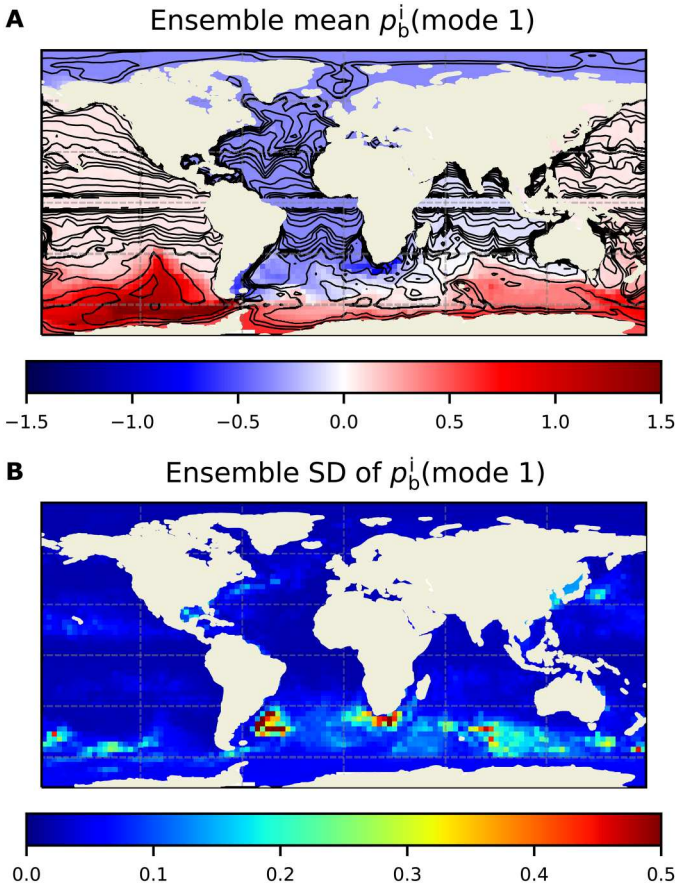

Fig. 1. Global-scale EOF mode 1 of p_b^i variability. Ensemble mean (**A**) and ensemble SD (**B**) of mode 1 p_b^i variability across the 50 ensemble members. Units are in centimeter, where we have converted p_b^i values to equivalent water thickness by dividing them by a reference sea water density and the acceleration of gravity, with 1 cm approximately equivalent to 1 hPa. Contours in (A) are lines of constant H/f [m·s].

is consistent with enhanced amplitude of mode 1 in the Bellingshausen-Amundsen basin and also around the Antarctic coast.

In contrast, anomalies on the Atlantic side adjust initially along South America and the equator through barotropic Kelvin wave propagation, followed by poleward propagation along the African and European coasts and into the Arctic. There is also adjustment from the eastern boundary through Rossby wave radiation along H/f contours (Fig. 1A). The end result is a quasi-equilibrium response with very weak p_b^i gradients in the Atlantic/Arctic basins (Fig. 1A), given the fast adjustment time scales and the large spatial scales of the wave processses.

Barotropic waves involved in the global adjustment are indeed quite fast. Long Rossby wave and Kelvin wave propagation speeds scale as βR^2 and $\sqrt{gH}$, respectively, where $\beta \sim 10^{-11}$ s$^{-1}m^{-1}$ is the Rossby parameter and $R \sim \sqrt{gH}/f \sim 2 \cdot 10^6$ m is the barotropic Rossby deformation radius (g is acceleration of gravity) (*27*, *28*). With propagation speeds on the order of 200 m/s (Kelvin) and 40 m/s (Rossby), signals can cross ocean basins in a few days, i.e., much shorter than a month, consistent with our findings of the global-scale p_b^i structure in Fig. 1.

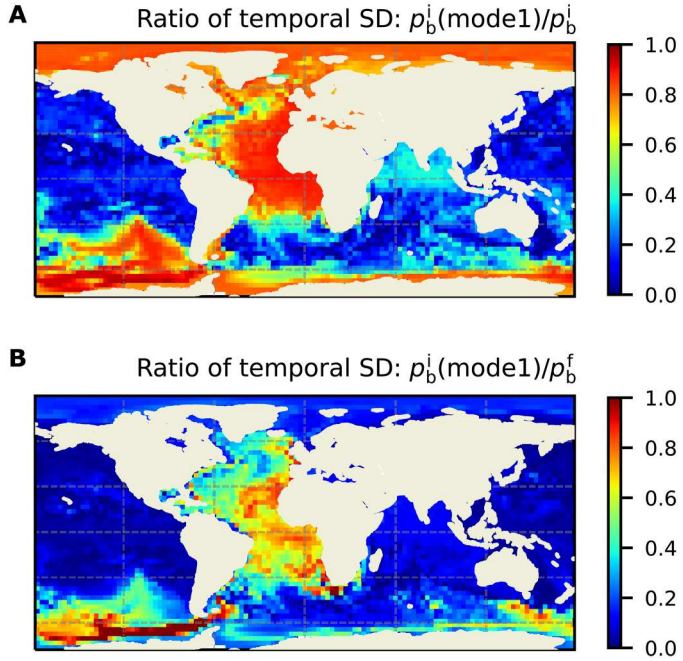

Fig. 2. Importance of mode 1 p_b^i variability. Ratio of the temporal SD of the mode 1 p_b^i to that of total p_b^i (**A**) and of p_b^f (**B**) using one arbitrary ensemble member.

In the Indian and Pacific oceans, mode 1 magnitudes are comparatively weak (Fig. 1A). We speculate that energy transmission from the Atlantic to the Indian Ocean around South Africa is not very efficient and that most of the energy propagating southward along the west coast of Africa ends up being scattered westward and staying in the Atlantic basin. Similarly, because westward propagating energy in the Southern Ocean is more confined to Antarctica, leakage of energy into the Pacific basin along the east coast of Australia is relatively weak. As a result, in both the Indian and Pacific oceans, mode 1 magnitudes can be substantially lower than those in the other basins.

Global-scale p_b^i pattern in GRACE observations

The total p_b variability in OCCIPUT is consistent with that inferred from GRACE and GRACE-FO data (fig. S2). Given the global scales and amplitudes involved, the p_b^i mode of variability derived from the OCCIPUT model analysis should be observable with GRACE and GRACE-FO measurements. Because there is no clear separation of scales between mode 1 and p_b^f, attempts to isolate this mode in the remotely observed p_b fields from those missions proved too challenging. Instead, to explore the presence of mode 1 in the GRACE observations, we compare the measured p_b variability (Fig. 3A) with two OCCIPUT-generated p_b fields: p_b^f (Fig. 3B) and p_b^f plus p_b^i from mode 1 (Fig. 3C).

Over most of the oceans, we find that adding p_b^i from mode 1 to p_b^f brings the SDs simulated by OCCIPUT closer to those estimated from GRACE (Fig. 3D). Regions with largest improvements to modeled p_b variability when adding p_b^i from mode 1 (e.g., the Bellingshausen-Amudsen basin) are coincident with the largest amplitudes in the mode 1 p_b^i pattern (Fig. 1A), which are considerably larger than the noise level in GRACE data. Results in Fig. 3 indicate that the global-scale p_b^i mode we identified from the model output is likely present in the observations.

DISCUSSION

Our findings show the notable large-scale impacts on the p_b field of random intrinsic processes. The global-scale p_b^i signature identified in this work is also reflected in the substantial p_b^i variations found in relatively quiet eddy areas, such as the eastern Atlantic Ocean (*16*). Our analyses indicate that such global-scale p_b^i variability can amount to at least half of p_b^f variability in those regions and can thus be important for understanding p_b variability in extensive ocean regions.

The existence of these global-scale pressure fluctuations from intrinsic processes in observations raises questions about being able to differentiate between p_b^i and p_b^f. This is particularly important when comparing or assimilating GRACE-like observations with coarse-resolution models, in which p_b is mostly driven by atmospheric forcing, and is also relevant for trying to understand ocean variability and predictability more generally. Separation of p_b^i and p_b^f variability might be a difficult task, however, given possible mingling spatiotemporal scales, as is the case with the p_b^i mode in Fig. 1A. We note that separating intrinsic from atmospherically driven signals discussed here is different from the topic of isolating anthropogenically forced signals from natural variability (*29*). The latter topic is potentially easier due to the distinct time scales in the two components.

Although the quasi-free global barotropic adjustment offers a plausible explanation for the basin-scale features of the p_b^i mode highlighted here, the detailed nature of the "noise maker" in the Drake Passage region remains to be described. Instabilities of the Antarctic Circumpolar Current fronts could lead to related anomalous currents and mass transports. Details of the interactions of the mean flows with topography could be important. Moreover, location of instabilities and associated mass anomalies relative to the coasts and the structure of H/f contours, including regions of closed contours, could help define propagation pathways and the nature of the large-scale adjustment. These issues merit future dedicated model studies involving more variables than just p_b analyzed here and assessing sensitivities to model settings.

MATERIALS AND METHODS

GRACE and GRACE-FO p_b data

We use monthly p_b data returned from GRACE and GRACE-FO missions and processed by the Jet Propulsion Laboratory (RL06M.MSCNv02). The GRACE/GRACE-FO data are available from April 2002 to present, with horizontal resolution of 3°. For comparison with OCCIPUT output, the linear trend of p_b from GRACE/GRACE-FO on each grid point is removed.

Isolating p_b^i from p_b^f using OCCIPUT output

Our analyses are based on the daily p_b output from 50 ensemble members from OCCIPUT (https://meom-group.github.io/projects/occiput/). The horizontal resolution is ~1/4°, providing NEMO-based eddy-permitting ocean/ice hindcasts over 1960–2015. The ensemble members are driven by the same 6-hourly realistic atmospheric forcing from atmospheric reanalyses (Drakkar

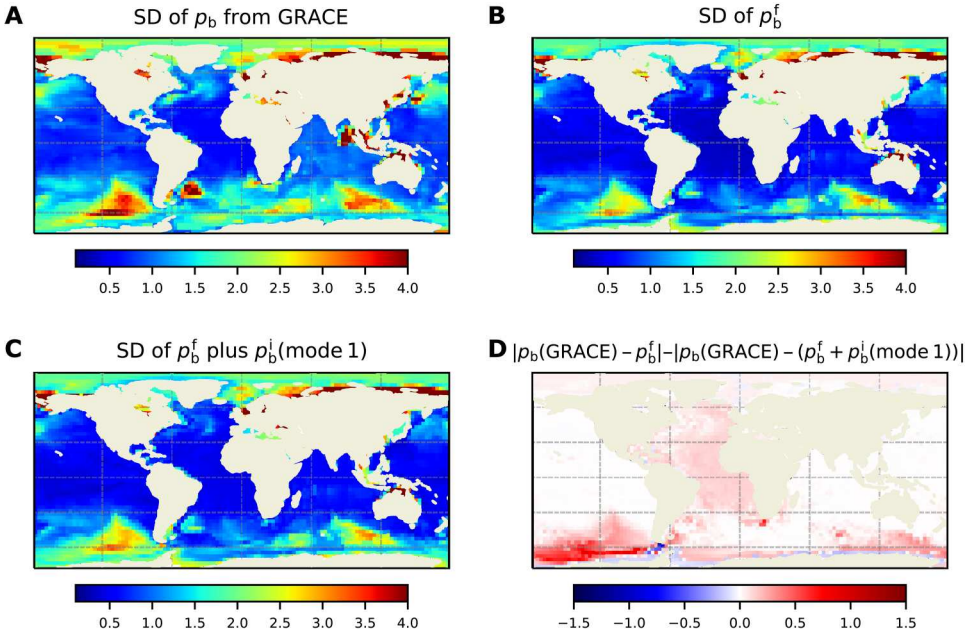

Fig. 3. Global-scale p_b^i in GRACE data. SD of p_b from GRACE (**A**), of p_b^f from OCCIPUT (**B**), and of p_b^f plus p_b^i from mode 1 (**C**) using one arbitrary ensemble member. (**D**) Difference between the absolute value of (A) minus (B) and that of (A) minus (C). Units for all panels are in centimeter, as in Fig. 1.

Forcing set DFS5.2). The linear trend of the p_b field is subtracted at each grid point within individual ensemble members to remove the potential contributions of model drift and geophysical tendencies and to focus on bottom pressure variability.

In this study, we analyze p_b over 2002–2015, the common period between OCCIPUT and GRACE. Daily, 1/4°-resolution p_b is first averaged to monthly and $3° \times 3^{\beta}$ cells to obtain $p_b(x, y, mon, mem)$, where (x, y) denotes the grid cell, *mon* means the month, and *mem* represents the ensemble member. We can then calculate p_b^f as the ensemble-mean pressure field $p_b^f(x, y, mon) = \sum_{mem=1}^{50} p_b(x, y, mon, mem)/50$. For individual ensemble members, p_b^i is estimated as $p_b^i(x, y, mon, mem) = p_b(x, y, mon, mem) - p_b^f(x, y, mon)$.

Supplementary Materials

This PDF file includes:

Supplementary Text
Figs. S1 and S2

REFERENCES AND NOTES

1. D. P. Chambers, J. Schröter, Measuring ocean mass variability from satellite gravimetry. *J. Geodyn.* **52**, 333–343 (2011).
2. G. C. Johnson, D. P. Chambers, Ocean bottom pressure seasonal cycles and decadal trends from GRACE Release-05: Ocean circulation implications. *J. Geophys. Res. Oceans* **118**, 4228–4240 (2013).
3. C. W. Hughes, J. Williams, A. Blaker, A. Coward, V. Stepanov, A window on the deep ocean: The special value of ocean bottom pressure for monitoring the large-scale, deep-ocean circulation. *Prog. Oceanogr.* **161**, 19–46 (2018).
4. D. L. Volkov, S.-K. Lee, F. W. Landerer, R. Lumpkin, Decade-long deep-ocean warming detected in the subtropical South Pacific. *Geophys. Res. Lett.* **44**, 927–936 (2017).
5. B. D. Tapley, S. Bettadpur, M. Watkins, C. Reigber, The gravity recovery and climate experiment: Mission overview and early results. *Geophys. Res. Lett.* **31**, 9607 (2004).
6. B. D. Tapley, M. M. Watkins, F. Flechtner, C. Reigber, S. Bettadpur, M. Rodell, I. Sasgen, J. S. Famiglietti, F. W. Landerer, D. P. Chambers, J. T. Reager, A. S. Gardner, H. Save, E. R. Ivins, S. C. Swenson, C. Boening, C. Dahle, D. N. Wiese, H. Dobslaw, M. E. Tamisiea, I. Velicogna, Contributions of GRACE to understanding climate change. *Nat. Clim. Change.* **9**, 358–369 (2019).
7. R. P. Kornfeld, B. W. Arnold, M. A. Gross, N. T. Dahya, W. M. Klipstein, P. F. Gath, S. Bettadpur, GRACE-FO: The Gravity Recovery and Climate Experiment Follow-On Mission. *J. Spacecr. Rockets.* **56**, 931–951 (2019).
8. F. W. Landerer, F. M. Flechtner, H. Save, F. H. Webb, T. Bandikova, W. I. Bertiger, S. V. Bettadpur, S. H. Byun, C. Dahle, H. Dobslaw, E. Fahnestock, N. Harvey, Z. Kang, G. L. H. Kruizinga, B. D. Loomis, C. McCullough, M. Murböck, P. Nagel, M. Paik, N. Pie, S. Poole, D. Strekalov, M. E. Tamisiea, F. Wang, M. M. Watkins, H.-Y. Wen, D. N. Wiese, D.-N. Yuan, Extending the global mass change data record: GRACE Follow-On instrument and science data performance. *Geophys. Res. Lett.* **47**, e2020GL088306 (2020).
9. K. J. Quinn, R. M. Ponte, Estimating weights for the use of time-dependent gravity recovery and climate experiment data in constraining ocean models. *J. Geophys. Res. Oceans* **113**, 10.1029/2008JC004903, (2008).
10. A. Köhl, F. Siegismund, D. Stammer, Impact of assimilating bottom pressure anomalies from GRACE on ocean circulation estimates. *J. Geophys. Res. Oceans* **117**, 10.1029/2011JC007623 (2012).
11. R. M. Ponte, A preliminary model study of the large-scale seasonal cycle in bottom pressure over the global ocean. *J. Geophys. Res.* **104**, 1289–1300 (1999).
12. V. N. Stepanov, C. W. Hughes, Propagation of signals in basin-scale ocean bottom pressure from a barotropic model. *J. Geophys. Res. Oceans* **111**, 10.1029/2005JC003450, (2006).
13. A. Carret, W. Llovel, T. Penduff, J.-M. Molines, Atmospherically forced and chaotic interannual variability of regional sea level and its components over 1993-2015. *J. Geophys. Res.* **126**, e2020JC017123 (2021).
14. H. Na, D. R. Watts, J.-H. Park, C. Jeon, H. J. Lee, M. Nonaka, A. D. Greene, Bottom pressure variability in the Kuroshio Extension driven by the atmosphere and ocean instabilities. *J. Geophys. Res. Oceans* **121**, 6507–6519 (2016).
15. C. W. Hughes, J. Williams, A. Hibbert, C. Boening, J. Oram, A Rossby whistle: A resonant basin mode observed in the Caribbean Sea. *Geophys. Res. Lett.* **43**, 7036–7043 (2016).
16. M. Zhao, R. Ponte, T. Penduff, S. Close, W. Llovel, J.-M. Molines, Imprints of ocean chaotic intrinsic variability on bottom pressure and implications for data and model analyses. *Geophys. Res. Lett.* **48**, e2021GL096341 (2021).
17. B. K. Arbic, R. B. Scott, G. R. Flierl, A. J. Morten, J. G. Richman, J. F. Shriver, Nonlinear cascades of surface oceanic geostrophic kinetic energy in the frequency domain. *J. Phys. Oceanogr.* **42**, 1577–1600 (2012).

18. B. K. Arbic, M. Müller, J. G. Richman, J. F. Shriver, A. J. Morten, R. B. Scott, G. Sérazin, T. Penduff, Geostrophic turbulence in the frequency–wavenumber domain: Eddy-driven low-frequency variability. *J. Phys. Oceanogr.* **44**, 2050–2069 (2014).
19. G. Sérazin, T. Penduff, B. Barnier, J.-M. Molines, B. K. Arcitc, M. Müller, L. Terray, Inverse cascades of kinetic energy as a source of intrinsic variability: A global OGCM study. *J. Phys. Oceanogr.* **48**, 1385–1408 (2018).
20. O. Arzel, T. Huck, Contributions of atmospheric stochastic forcing and intrinsic ocean modes to North Atlantic ocean interdecadal variability. *J. Climate* **33**, 2351–2370 (2020).
21. A. Hochet, T. Huck, O. Arzel, F. Sévellec, A. C. D. Verdière, M. Mazloff, B. Cornuelle, Direct temporal cascade of temperature variance in eddy-permitting simulations of multidecadal variability. *J. Climate* **33**, 9409–9425 (2020).
22. T. Penduff, B. Barnier, L. Terray, L. Bessières, G. Sérazin, S. Gregorio, J.-M. Brankart, M.-P. Moine, J.-M. Molines, P. Brasseur, Ensembles of eddying ocean simulations for climate. *CLIVAR Exchanges* **19**, 26–29 (2014).
23. L. Bessières, S. Leroux, J.-M. Brankart, J.-M. Molines, M.-P. Moine, P.-A. Bouttier, T. Penduff, L. Terray, B. Barnier, G. Sérazin, Development of a probabilistic ocean modelling system based on NEMO 3.5: Application at eddying resolution. *Geosci. Model Dev.* **10**, 1091–1106 (2017).
24. J.-M. Brankart, Impact of uncertainties in the horizontal density gradient upon low resolution global ocean modelling. *Ocean Model.* **66**, 64–76 (2013).
25. J.-M. Brankart, G. Candille, F. Garnier, C. Calone, A. Melet, P.-A. Bouttier, P. Brasseur, J. Verron, A generic approach to explicit simulation of uncertainty in the NEMO ocean model. *Geosci. Model Dev.* **8**, 1285–1297 (2015).
26. S. Close, T. Penduff, S. Speich, J.-M. Molines, A means of estimating the intrinsic and atmospherically-forced contributions to sea surface height variability applied to altimetric observations. *Progress in Oceanogr.* **184**, 102314 (2020).
27. A. E. Gill, *Atmosphere-Ocean Dynamics* (Academic Press, 1982).
28. G. K. Vallis, *Atmospheric and Oceanic Fluid Dynamics* (Cambridge University Press, 2017).
29. B. D. Hamlington, J. T. Fasullo, R. S. Nerem, K.-Y. Kim, F. W. Landerer, Uncovering the pattern of forced sea level rise in the satellite altimeter record. *Geophys. Res. Lett.* **46**, 4844–4853 (2019).

Acknowledgments: The OCCIPUT ensemble simulation was achieved using the PRACE Research Infrastructure resource CURIE based in France at TGCC. We thank J.-M. Molines and L. Bessiéres from CNRS for conducting the OCCIPUT ensemble simulations and maintaining model output. **Funding:** This study is funded by NASA through GRACE Follow-On Science Team Grant 80NSSC20K0728 to AER. This work is a contribution to the OCCIPUT and IMHOTEP projects. OCCIPUT has been funded by ANR through contract ANR-13-BS06-0007-01. IMHOTEP is being funded by CNES through the Ocean Surface Topography Science Team (OST/ST).
Author contributions: M.Z. initiated and R.M.P. led this work. T.P. conducted and coordinated OCCIPUT ensemble simulations. Data processing and visualization were carried out by M.Z. under the guidance of R.M.P. The initial manuscript was written by M.Z. and R.M.P. and edited by T.P. All authors discussed the results and contributed to the final manuscript. **Competing interests:** The authors declare that they have no competing interests. **Data and materials availability:** All data needed to evaluate the conclusions in the paper are present in the paper and/or the Supplementary Materials. The GRACE data and OCCIPUT p_b fields, which are averaged onto the same $3° \times 3^{\beta}$ grids, are available at https://zenodo.org/record/7833830#.ZDwdpezMKWY.

Submitted 28 November 2022
Accepted 21 June 2023
Published 21 July 2023
10.1126/sciadv.adg0278

ScienceAdvances

Global-scale random bottom pressure fluctuations from oceanic intrinsic variability

Mengnan Zhao, Rui M. Ponte, and Thierry Penduff

Sci. Adv., **9** (29), eadg0278.
DOI: 10.1126/sciadv.adg0278